Supplement for

Gas-Particle Partitioning of Semivolatile Organic Compounds When Wildfire Smoke Comes to Town

Yutong Liang*, Rebecca A. Wernis, Kasper Kristensen, Nathan M. Kreisberg, Philip L. Croteau, Scott C. Herndon, Arthur W.H. Chan, Nga L. Ng, Allen H. Goldstein*

Emails: Yutong Liang (yutong.liang@berkeley.edu); Allen Goldstein (ahg@berkeley.edu)

This Supplement contains:

S1. SV-TAG and cTAG chemical analysis and QA/QC

In both SV-TAG and cTAG, following collection of aerosol on the filter cells, the analytes were thermally desorbed in helium saturated with N-methyl-N-(trimethylsilyl) trifluoroacetamide (MSTFA) to convert the -OH groups of the SVOCs into -OSi$(CH_3)_3$ groups, which makes them less polar and better suited for the non-polar GC columns. After passing through the GC, analytes were detected by the mass spectrometer. Figure S1 shows representative total ion chromatograms of the bypass and denuded samples for the wildfire period and background period.

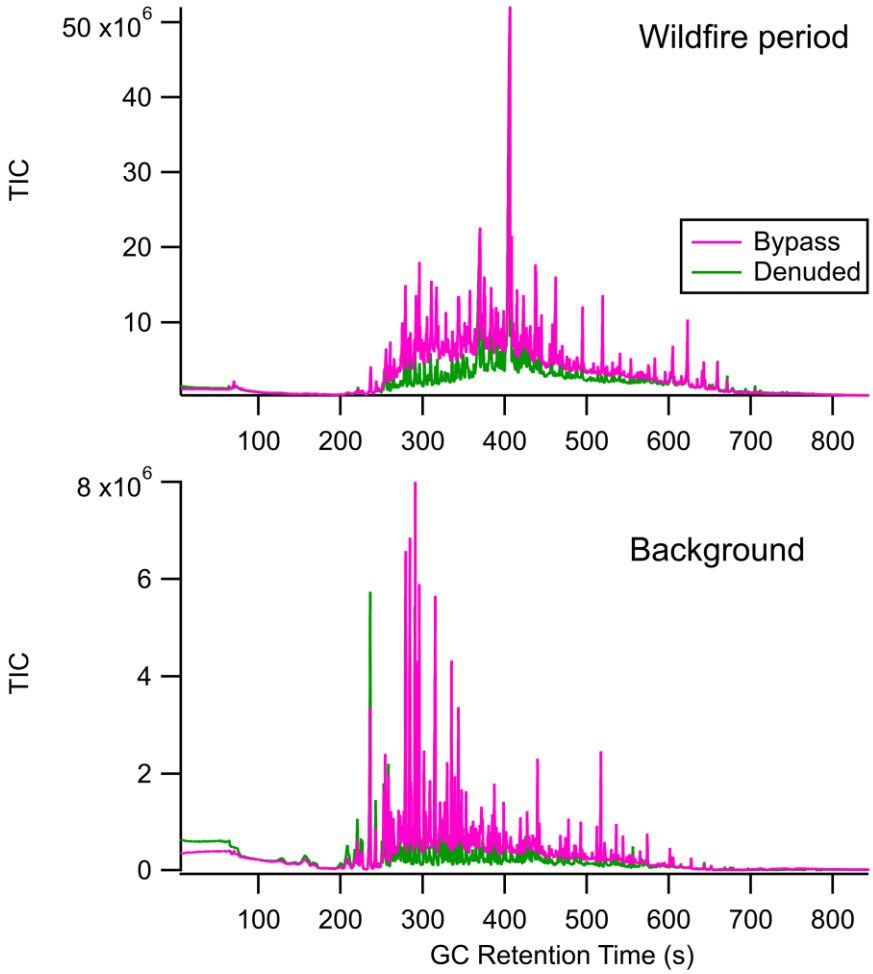

Figure S1. Total Ion Chromatogram of a wildfire sample and a background sample. GC retention time has a negative association with volatility (Isaacman-VanWertz et al., 2016).

Chromatographic data were analyzed using the TERNinIgor software by fitting the single ion peaks (Isaacman-VanWertz et al., 2017). A constant amount of isotopically labeled internal standards were injected to correct for drifts in instrument response, and known amounts of a mix of 99 compounds (Jen et al., 2019; Liang et al., 2021) were injected as standards for quantification purpose. Compounds were identified by matching with standard, the NIST 2020 mass spectral library, custom libraries made in previous studies (Jen et al., 2019; Zhang et al., 2018; Yee et al., 2018), and the mass spectra of filter samples collected outside the same building during the 2017 Northern California wildfires (Liang et al., 2021). We only considered compounds detected in at least 20% of the samples (only 4 out of the 89 compounds considered are present in less than 50% of samples in the 2017 Northern California dataset). More information about materials and methods is in Table S1.

Method blanks were performed by injecting deuterated internal standard to the cells. We determined the background signals of the compounds and calculated the ratio of background signal to mean bypass signal. Compounds with background-to-bypass signal larger than 10% (such as biphenyl and salicylic acid) were not considered in the analyses. There were another two compounds with background-to-bypass ratios larger than or equal to 5% (5.0% for catechol and 9.0% for 4-hydroxybenzoic acid). They were still included in the analysis. The same criterion is applied for the FIREX-AQ 2018 dataset, and fluoranthene was excluded from the analysis as a result. In addition, bypass signal data below the 3×background signal of each compound were not included in the analysis, while denuded signal data within this limit were kept.

For SV-TAG measurement, because two cells were used for sampling, the cell-to-cell bias needs to be accounted for. During sampling, the role of the two cells were swapped with each sample. For instance, if Cell 1 sampled gas + particle and Cell 2 sampled particle in Hour 1, then in Hour 2, Cell 1 would sample particle while Cell 2 would sample gas + particle. In addition, we collected 11 bypass samples simultaneously on two cells as a direct comparison during this campaign. Linear regression of the internal-standard-normalized signals of each compound measured from the two cells were performed, and the best-fit slopes were used to correct for the cell difference for each compound. More details can be found in Isaacman et al. (2014) and its Supplement.

The carryover from cell to cell can cause a positive bias to measured F_p. The magnitude of carryover has been systematically studied in Kreisberg et al. (2014). The carryover of total ion chromatogram was found to be 2.6 ± 0.1% and the median carryover of individual ions was found to be 2.4%. We can estimate the effect of carryover on F_p and C* as follows:

The real gas-phase fraction of a compound $F_{p\text{-}real}$ can be expressed as:

$$F_{p-real} = \frac{C_{g-real}}{C_{(g+p)-real}} \qquad \text{(Eq. S1)}$$

Assume the carryover of the compound is 2.6%. Then the measured gas-phase fraction ($F_{p\text{-}meas}$) can be expressed as:

$$F_{p-meas} = \frac{C_g + C_{g+p} \times 0.026}{C_{g+p} + C_g \times 0.026} = \frac{F_{p-real} + 0.026}{0.026 F_{p-real} + 1} \qquad \text{(Eq. S2)}$$

We can then plot $F_{p\text{-}real}$ and (uncorrected C* / corrected C*) as functions of $F_{p\text{-}meas}$. This ratio is the same as the bias of γ.

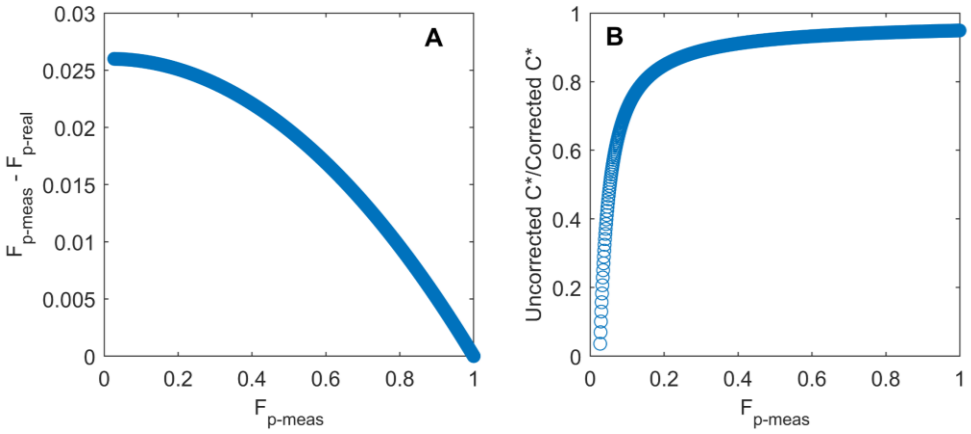

Figure S2. A. Overestimation of F_p because of carryover, as a function of $F_{p\text{-}meas}$; **B.** the ratio of inferred C* (without correction from carryover) over inferred C* (after correction of carryover), as a function of $F_{p\text{-}meas}$.

As Figure S1 suggests, the effect of carryover on F_p is negligible. However, when $F_{p\text{-}meas}$ is less than 0.05, C* can be underestimated by a factor of ½. When $F_{p\text{-}meas}$ is less than 0.03, C* can be underestimated by an order of magnitude. Therefore, compounds with median F_p less than 0.05 were not included in activity coefficient analysis.

Table S1. Materials and Methods for SV-TAG and cTAG (SV channel only) analysis

	SV-TAG	**cTAG**
Denuder	MAST Carbon, 500 channels, 30 mm outer diameter × 40.6 cm length	MAST Carbon, 500 channels, 30 mm outer diameter × 40.6 cm length (same as SV-TAG)
Collection and thermal desorption temperatures	30°C, 320°C	30°C, 315°C
GC and column	Agilent 7890A; Rtx-5Sil MS, 20 m × 0.18 mm × 0.18 µm (Restek)	Miniature GC; metal MXT-5, 20 m, 0.18mm i.d., 2µm phase thickness (Restek)
GC method	23.6 °C min^{-1} ramp from 50°C to 330°C, 2.2 min hold at 330°C in Helium.	1 min hold at 50°C, 20 °C min^{-1} ramp to 330°C, 4 min hold at 330°C in Helium.
Mass spectrometer	Agilent 5975C, EI, -70 eV	TOFWERK HR MS, EI, -70 eV

S2. Liquid vapor pressure estimation

The subcooled liquid vapor pressures were estimated by two group contribution models, i.e., the SIMPOL model and the EVAPORATION model (which only works for non-aromatic compounds) (Pankow and Asher, 2008; Compernolle et al., 2011). For the compounds considered here, we found that the predictions from the two models agree well with each other. The linear regression between $\log_{10}(P_{SIMPOL})$ and $\log_{10}(P_{EVAPORATION})$ yields and R^2 of 0.97 and root mean square error of 0.44. Such a difference did not meaningfully change any of our results. Therefore, the results presented in this manuscript are based on vapor pressures estimated by the SIMPOL model. In addition, similar to our previous work, we used the MPBPWIN component (modified Grain method) in EPA's EPI Suite (US EPA, 2012) to estimate the vapor pressures of nitro-aromatic compounds, because the SIMPOL model substantially overestimate the vapor

pressures of these compounds in general (Bannan et al., 2017; Wania et al., 2017). The saturation vapor pressure $v_{P,i}$ (in Pa) of each compound was converted to the saturation mass concentration over pure compound *i*, C_i^O at 298K by:

$$C_i^O = \frac{v_{P,i} \mathrm{MW}_i}{RT} \quad \text{(Eq. S3)}$$

where R is the gas constant (8.314 J mol^{-1} K^{-1}), T is the temperature, 298K. MW_i is the molecular weight of compound *i* in g mol^{-1}. C_i^O was then converted into μg m^{-3}.

For Figure 2, the effective saturation mass concentration of compound *i* (C_i^*) at a given temperature was converted to 298K values using the Clausius-Clapeyron Equation(Epstein et al., 2010):

$$C_i^*(298K) = C_i^*(T) \exp[\frac{\Delta H_{vap,i}}{R}(\frac{1}{T} - \frac{1}{298K})]\frac{T}{298K} \quad \text{(Eq. S4)}$$

where $\Delta H_{vap,i}$ is the enthalpy of vaporization of compound *i*, T is the temperature in Kelvin. The enthalpy data were taken from the NIST Webbook (NIST, 2022), May et al. (2012), or estimated by the equation in May et al. (2013) and Thornton et al. (2020) (and take average) when measured data were not available.

S3. Estimation of O/C and H/C ratios, H^+, and aerosol liquid water content (ALWC)

In the FIREX-AQ 2018 study, the O/C ratio and H/C ratios were estimated from the fractions of *m/z* 44 and *m/z* 43 signals in the total organic signal measured by the ACSM, following the parametrizations by Aiken et al. (2008) and Ng et al. (2011), respectively.

The mass concentration of H^+ in the particle phase of particle per unit volume of air was estimated by assuming charge neutrality (Zhang et al., 2007):

$$H^+ = 2 \times SO_4^{2-} / 96 + NO_3^- / 62 + Cl^- / 35.5 - NH_4^+ / 18 \quad \text{(Eq. S5)}$$

where SO_4^{2-}, NO_3^-, Cl^-, and NH_4^+ are the mass concentrations of the aerosol components measured by the ACSM.

The total ALWC is the sum of the inorganic water content caused by inorganic ions, and the organic water content caused by the uptake of water by the hygroscopic organic aerosol. The

inorganic water content was estimated using the ISOPORRIA-II model (Fountoukis and Nenes, 2007) in reverse mode, assuming a metastable phase state, following the settings by Isaacman-VanWertz et al. (2016). The organic water content was estimated following the approach by Guo et al. (2015).

$$W_O = M_{Org} \frac{\rho_{Org}}{\rho_W} \frac{\kappa_{Org}(\mathrm{O/C})}{\frac{100}{RH\%} - 1} \qquad \text{(Eq. S6)}$$

where M_{Org} is the mass concentration of organic aerosol measured by the ACSM, ρ_{Org} and ρ_W are the densities of organic aerosol and water, respectively. RH is the relative humidity. The estimation of O/C ratio is described above. The organic hygroscopicity parameter κ_{Org} is assumed to be 0.2 for aged BBOA (Engelhart et al., 2012). Due to the low RH during the wildfire season, the aerosol water content caused by organic aerosol dominated the total aerosol liquid water content (mean ± standard deviation = 74% ± 15%).

S4. AIOMFAC simulations

To elucidate the effect of BBOA on the partitioning behavior of urban SVOCs observed in Berkeley, we calculated the activity coefficients (γ) using the Aerosol Inorganic-Organic Mixtures Functional groups Activity Coefficients (AIOMFAC) model (Zuend et al., 2011). Since we did not have bulk composition measured, aerosol compositions from relevant studies in literature were used. We parsimoniously assumed that the aerosol measured on campus was composed of urban OA, BBOA, and water. Inorganic species were ignored. The urban aerosol composition (cooking OA, hydrocarbon-like OA (HOA), and less-oxidized oxygenated organic aerosol (LOOOA)) was taken from a mobile measurement study in Oakland, California (a city adjacent to Berkeley) (Shah et al., 2018). The surrogate compound for cooking OA was based on Faber et al. (2017). The BBOA surrogates were taken from Pye et al. (2018). with the addition of dehydroabietic acid. We performed two sets of simulations, with the aerosol components and their mass fractions shown in Table S2. In the High RH set of simulations, we assumed that 10% of aerosol was water. We increased the mass fraction of BBOA from 6% to 86% of total aerosol, while the mass fraction of urban OA decreased from 84% of total aerosol to 4% of total aerosol. The resulting RH was 78% to 39% from urban OA dominance to BBOA dominance. In the low RH case, we assumed the mass fraction of water to be 5% of total aerosol, increased the BBOA

from 11% to 91% while decreased the urban OA from 84% to 4%. The resulting RH in the low RH case was 45% to 19% from urban OA dominance to BBOA dominance.

Table S2. Aerosol components, surrogate structures, O/C ratio of the surrogate structures and the mass fractions of the aerosol components used in the AIOMFAC simulations.

Aerosol component	**Surrogate in AIOMFAC**	**O/C**	**Amount by mass**
Cooking OA	$(CH_3)_2(CH_2)_{13}(CH_2^{[OH]})(CH{=}CH)(COOH)(OH)$	0.16	0.6×LOOOA
HOA	$(CH_3)_2(CH_2)_{18}$	0	0.4×LOOOA
LOOOA	$(CH_3)_2(CH_2)(CH)(CH_2^{[OH]})_2(CH^{[OH]})(C^{[OH]})(OH)_4$	0.5	42%-2% of total aerosol
BBOA w/o levoglucosan	$(CH_2)(CH)(CH^{[OH]})_2(CH_2O)(CHO[ether])(OH)_2$	0.67	6%-83% of total aerosol
Levoglucosan	Levoglucosan	0.83	0.03×BBOA w/o levoglucosan
Dehydroabietic acid	Dehydroabietic acid	0.1	0.005×BBOA w/o levoglucosan
Water	Water	$+\infty$	Remaining 10% (5% in the low RH runs)

S5. Random forest model for the temporal variations of F_p

We tried to use random forest models to find out what are the most important factors controlling the temporal variations of the partitioning behaviors of individual SVOCs. We sought to use various measured variables, such as temperature and relative humidity (predictors) to predict the time series of F_p of individual compounds (response). Random forest algorithm, developed by Leo Breiman (Breiman, 2001), is an ensemble approach that makes prediction of the response using the aggregation of multiple decision trees. We used the bootstrap aggregation (bagging) method, in which each decision tree in the ensemble was trained on a random subset of the samples (with replacement), and the prediction results from the individual decision trees were then averaged to make more accurate predictions. This approach reduces the chance of overfitting by individual decision trees and therefore enhances prediction accuracy (Mecikalski et al., 2021). It can also be used to evaluate the importance of predictor variables on their contribution in predicting the response variable.

The random forest model was implemented with MATLAB 2022a, using 200 learning cycles. We set the number of predictors to select for each split to "*all*" to use all available predictors. The "*interaction-curvature*" algorithm was used to select the best split predictor at each node, and we allowed the use of the best surrogate predictor when the observation of a predictor is missing. We used the permutation of out-of-bag predictor observations method in MATLAB ("oobPermutedPredictorImportance" function) to rank the importance of predictors (MathWorks, 2022). Drawing N observations out of N observations with replacement will on average leave 37% of observations not being used to train the model (Breiman, 1996). These observations are out-of-bag observations. For each predictor variable x_j, we randomly permuted the out-of-bag observations of x_j, used trained model to predict the response (response is not permuted), and estimated the model error ε. This error was then compared with the model error of prediction using the unpermuted data. If the model performance significantly deteriorated when predictor *j* was permuted, then this variable is important. Otherwise this predictor variable is unimportant, or the information in this predictor variable has been contained in other predictor variables (McGovern et al., 2019). The higher the importance score is, the more important the factor is. Importance scores close to 0 mean low importance, and negative importance scores mean the model is accidentally better in using the permuted data to predict the response, which also means

the factor is not important. This is more likely to happen with relatively small datasets such as our F_p dataset (N = 112 data points for the 2017 Northern California dataset and N = 88 data points for the FIREX-AQ 2018 dataset, in which all predictor variables were measured).

S6. Supplementary figures

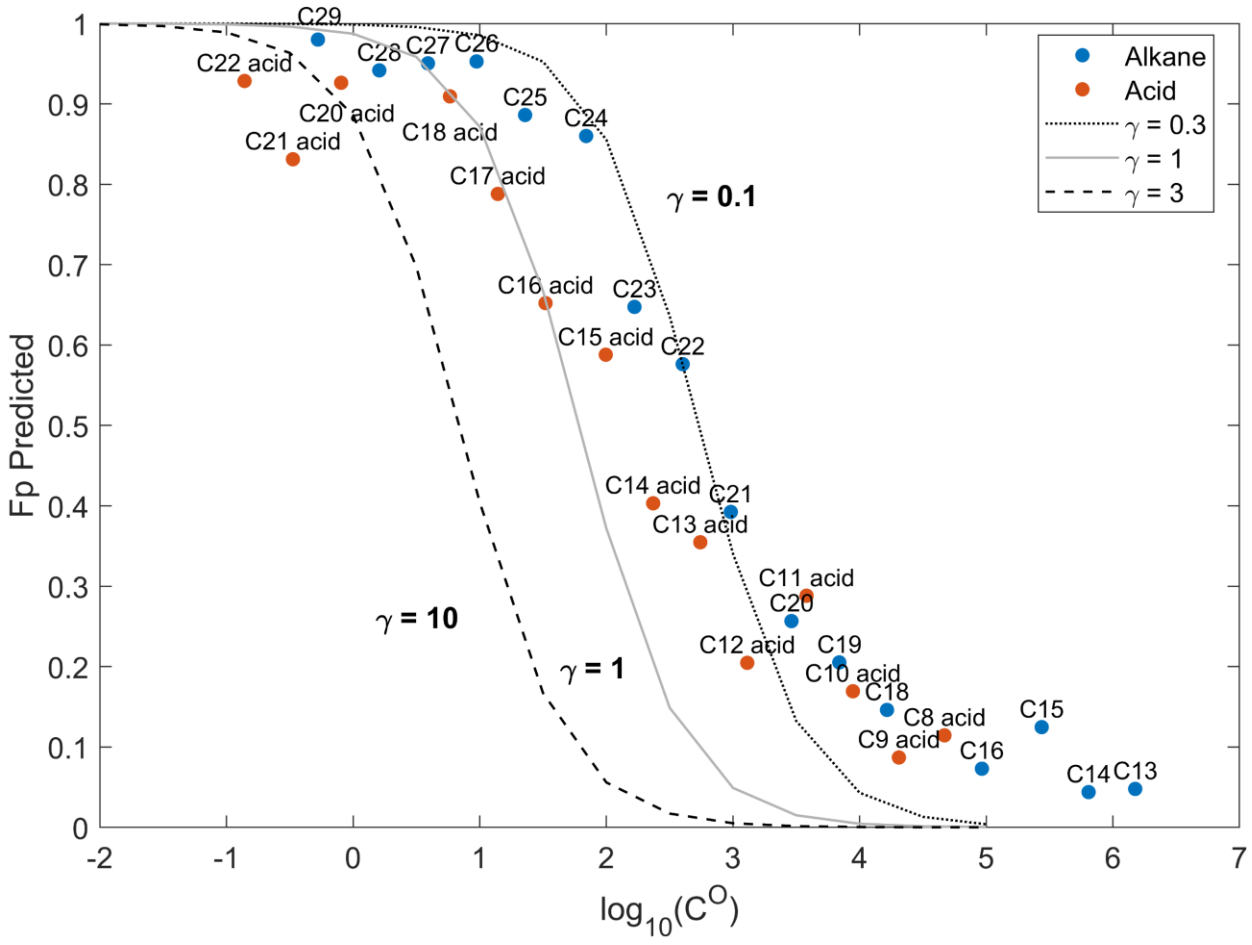

Figure S3. Measured and predicted F_p for *n*-alkanes and *n*-carboxylic acids, against the $\log_{10}C^O$ at 298K in the 2017 Northern California wildfires study. C13-C15 alkanes deviate from others probably because of potential interference such as decomposition of larger molecules or the carryovers from the gas + particle measurements of the previous time step, which may have a stronger effect on the particle-phase measurements of the light alkanes (whose signals are low).

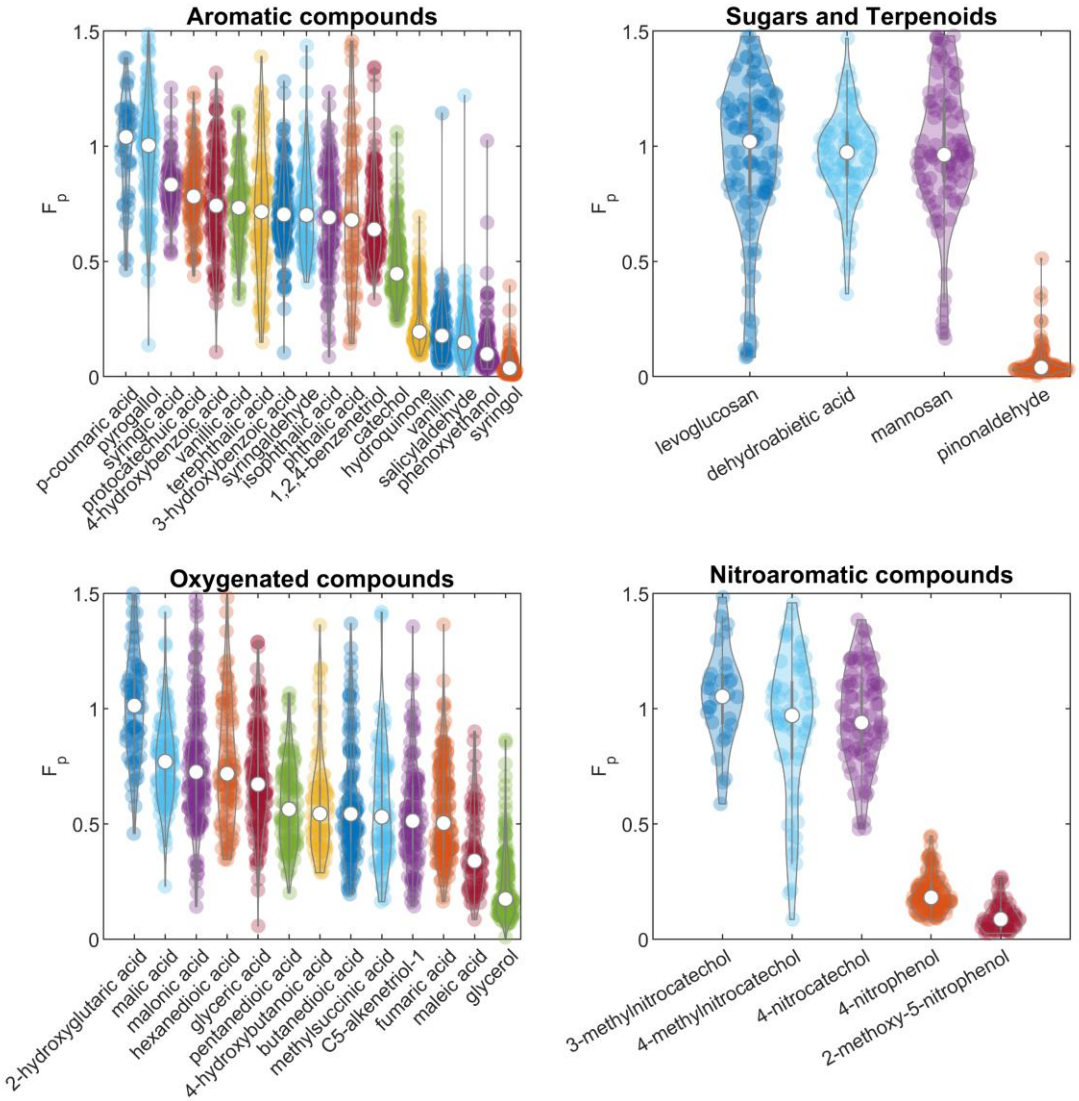

205 **Figure S4.** Violin plot of F_p of compounds in several classes in the 2017 Northern California wildfires study, showing interquartile range with whiskers extended to 1.5 times the interquartile range. Circles on each violin indicate the median. Compounds are ordered by descending median F_p.

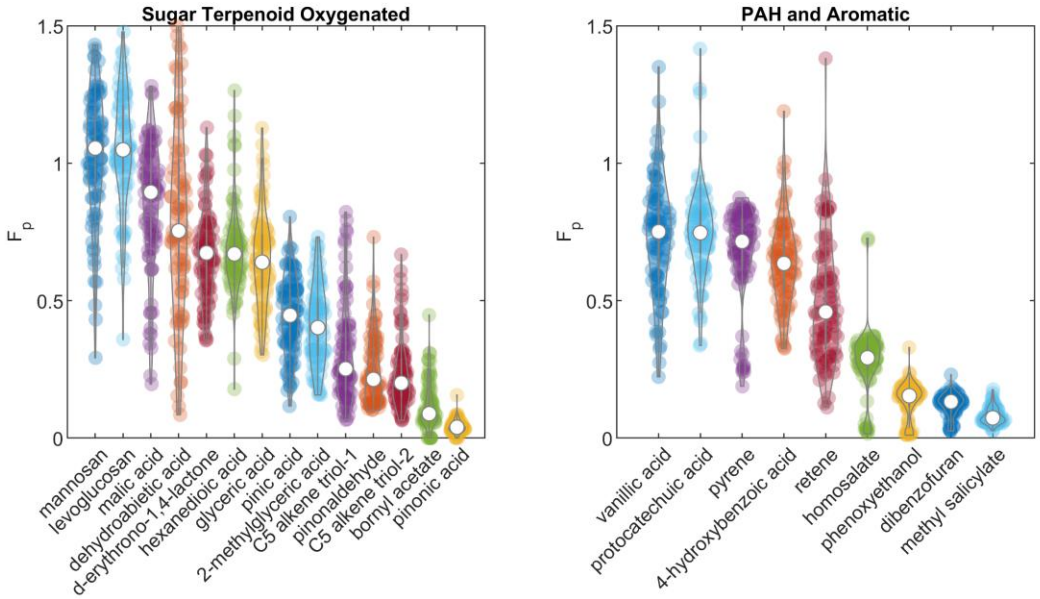

210 **Figure S5.** Violin plot of F_p of compounds in several classes in the FIREX-AQ 2018 study, showing interquartile range with whiskers extended to 1.5 times the interquartile range. Circles on each violin indicate the median. Compounds are ordered by descending median F_p.

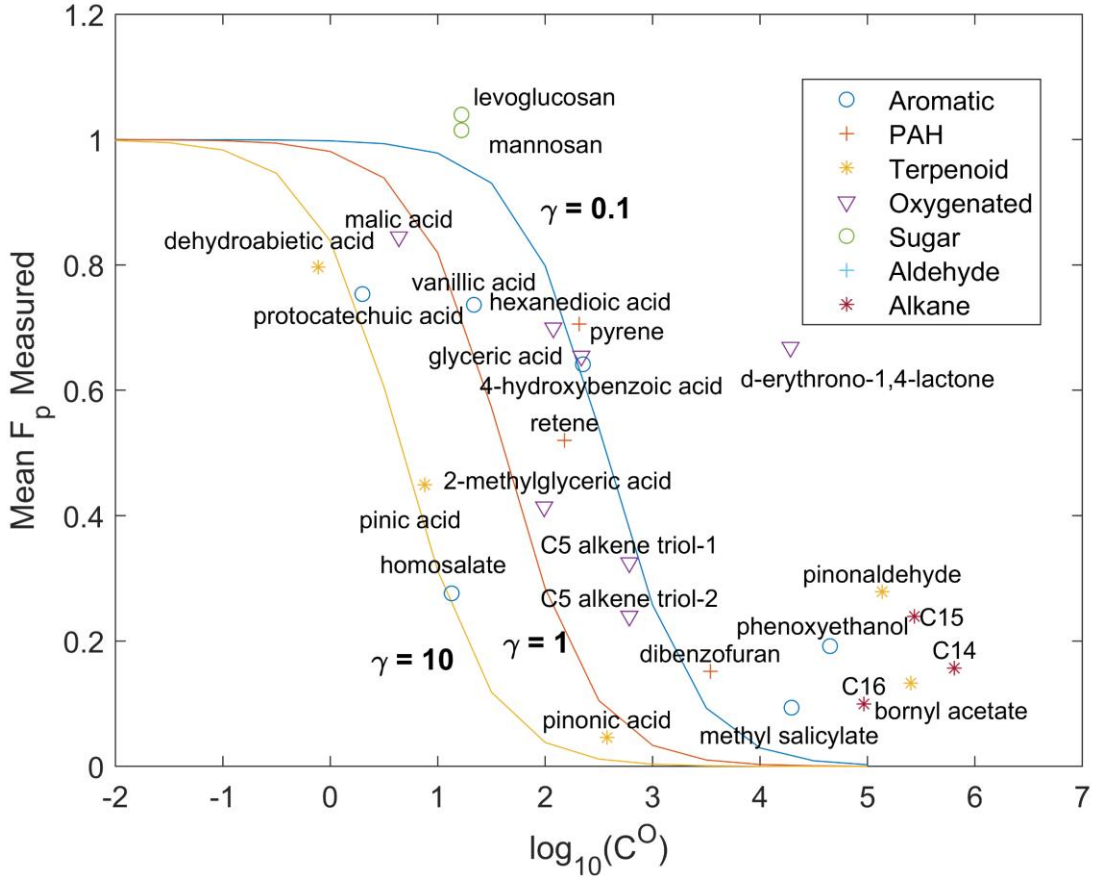

Figure S6. Campaign average F_p during the FIREX-AQ 2018 study, measured by the cTAG, classified by functional groups, plotted against their saturation concentration at 298K. Three curves on the figure are the theoretical particle fractions (F_p) predict from equilibrium absorptive partitioning model, assuming different activity coefficients (γ). The abnormally high F_p of d-erythrono-1,4-lactone (and its structure) suggests it is likely a fragmentation product of a lower volatility compound.

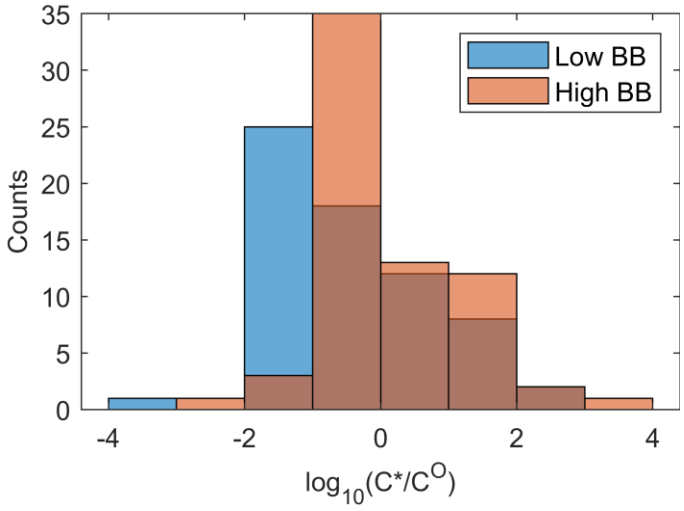

Figure S7. The logarithmic of effective saturation concentration over the pure saturation concentration, which is equivalent to the activity coefficient γ. Data are from the October 2017 Northern California wildfires campaign.

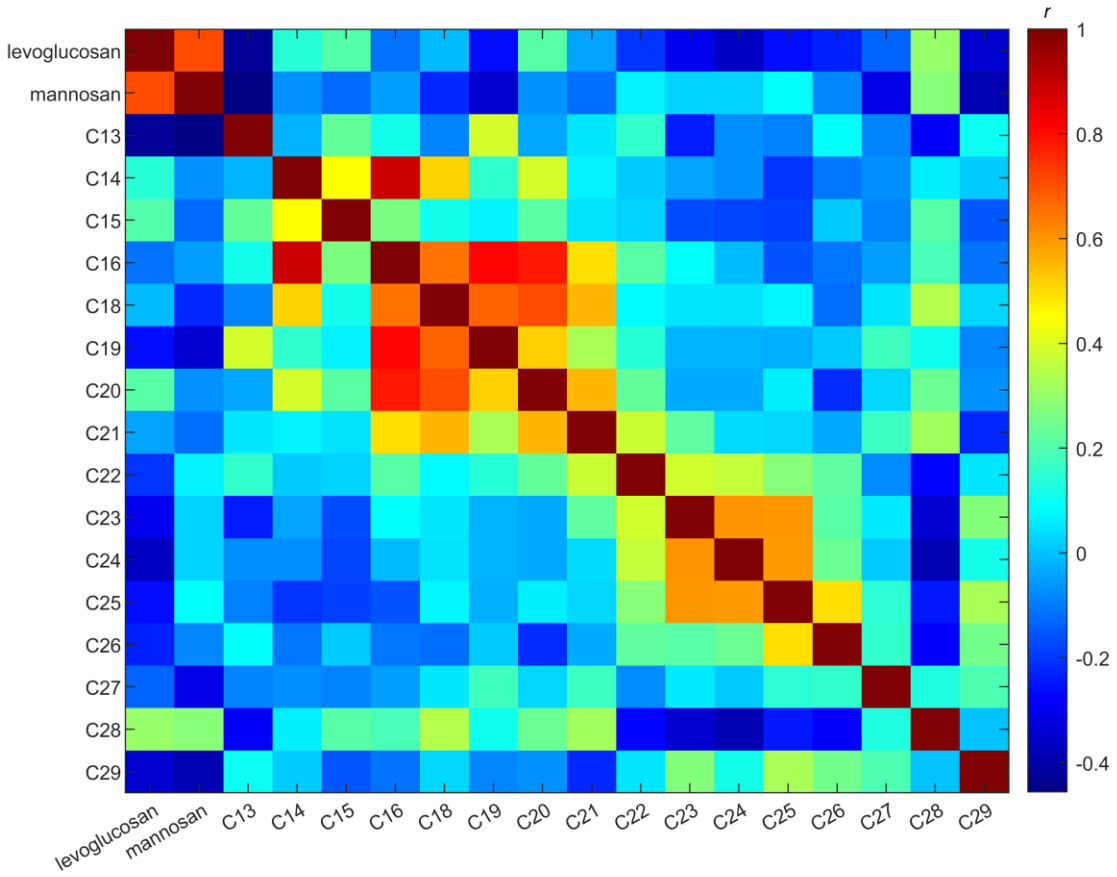

Figure S8. Correlation matrix of F_p time series for alkanes observed by SV-TAG in Berkeley, California during the October 2017 Northern California wildfires study.

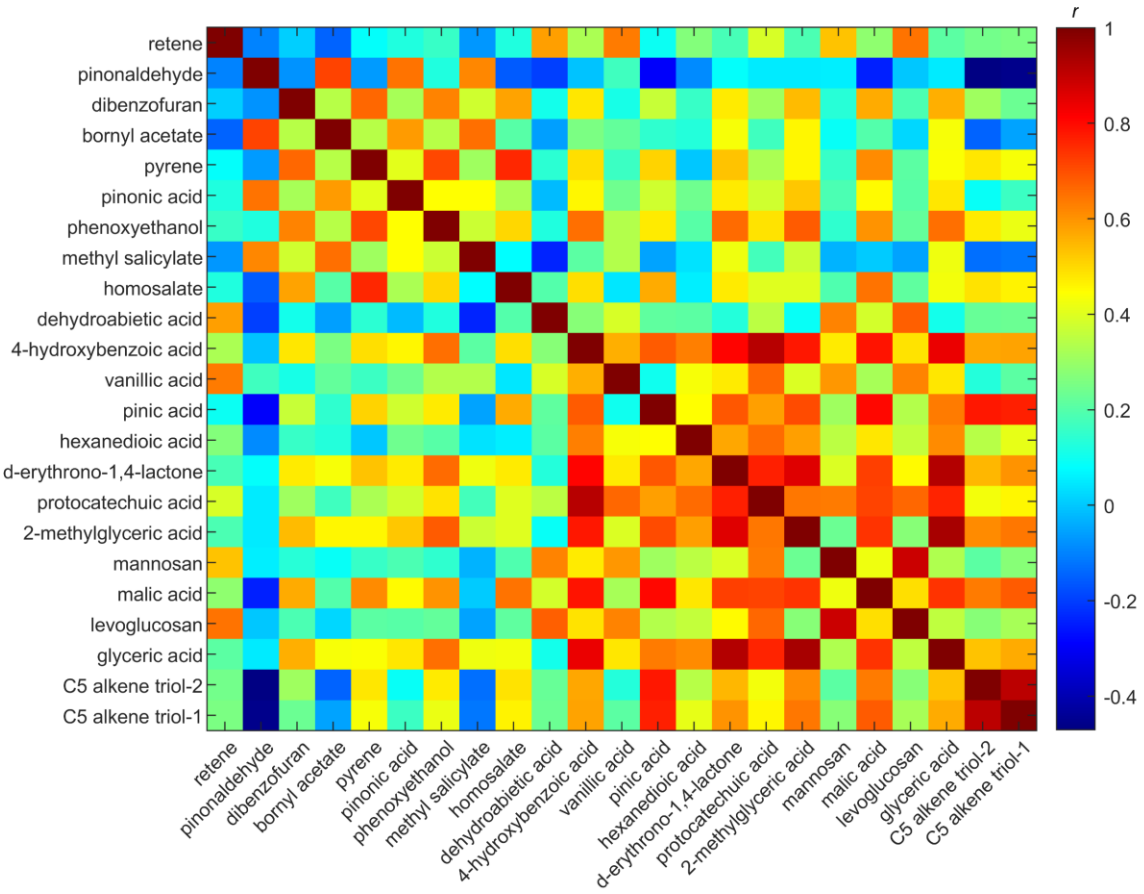

230 **Figure S9.** Correlation matrix of F_p time series for compounds observed by the cTAG in McCall, Idaho during the FIREX-AQ 2018 study. Compounds are ordered by the number of -OH groups in the molecules.

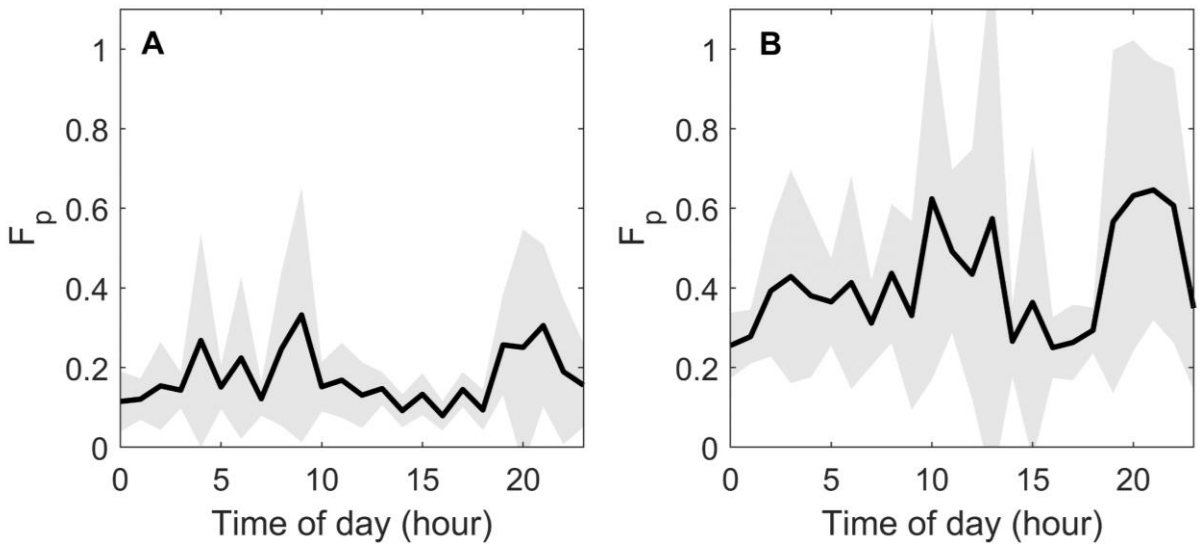

Figure S10. Diel profile of **A.** methyl palmitate and **B.** methyl stearate in Berkeley. Solid lines show the mean and shadings show the standard deviation.

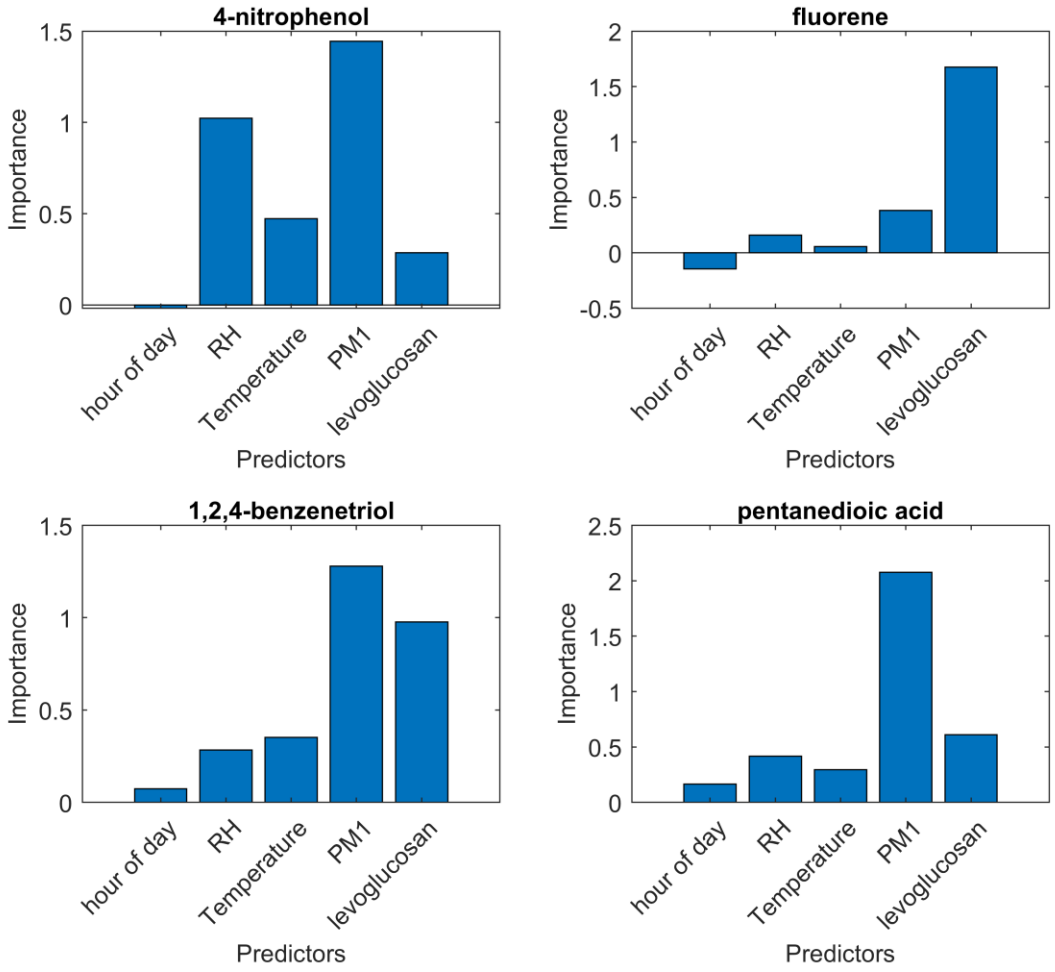

Figure S11. The importance scores of factors on the F_p of selected compounds, measured in the 2017 Northern California wildfires study. F_p of fluorene is negatively affected by the concentration of levoglucosan. F_p of all the compounds is positively affected by the concentration of PM_1.

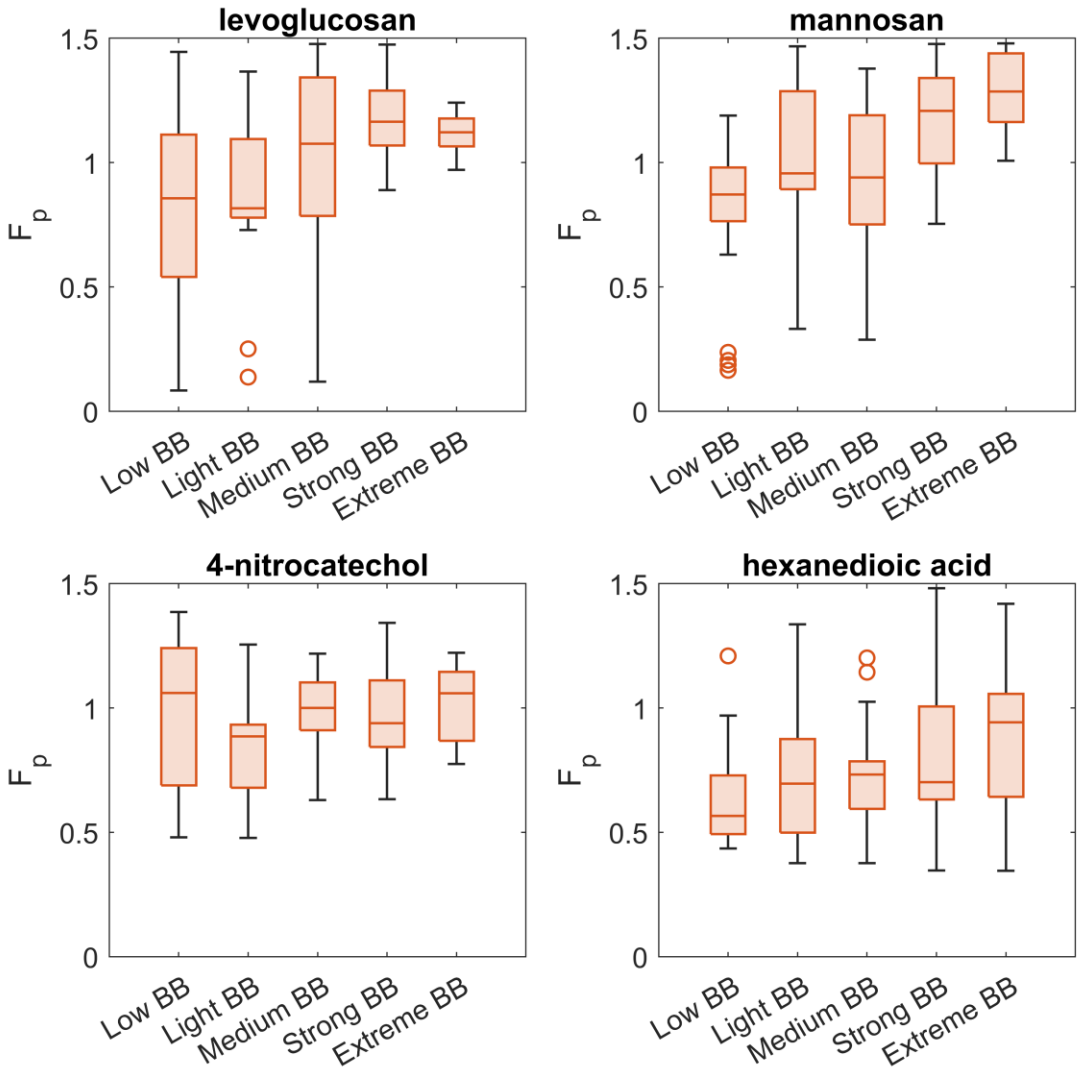

Figure S12. Boxplots showing the effect of BBOA on the particle phase fraction on selected polar compounds observed in the 2017 Northern California wildfires study. Each box plot shows the interquartile range with whiskers extended to 1.5 × the interquartile range. Central horizontal lines show the medians. Circles denote outliers.

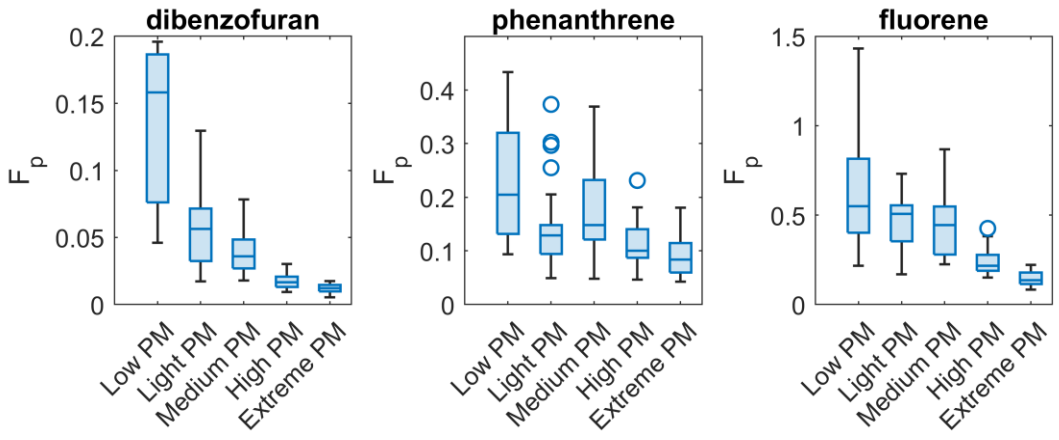

Figure S13. Boxplots showing the effect of BBOA on the particle phase fraction on selected polar compounds observed in the 2017 Northern California wildfires study. Each box plot shows the interquartile range with whiskers extended to 1.5 × the interquartile range. Central horizontal lines show the medians. Circles denote outliers. PM categories are based on the concentration of PM_1. Low PM: 0-40th percentile; light PM: 40th-60th percentile, medium PM: 60th-75th percentile, high to extreme PM: above 90th percentile of PM_1 concentration.

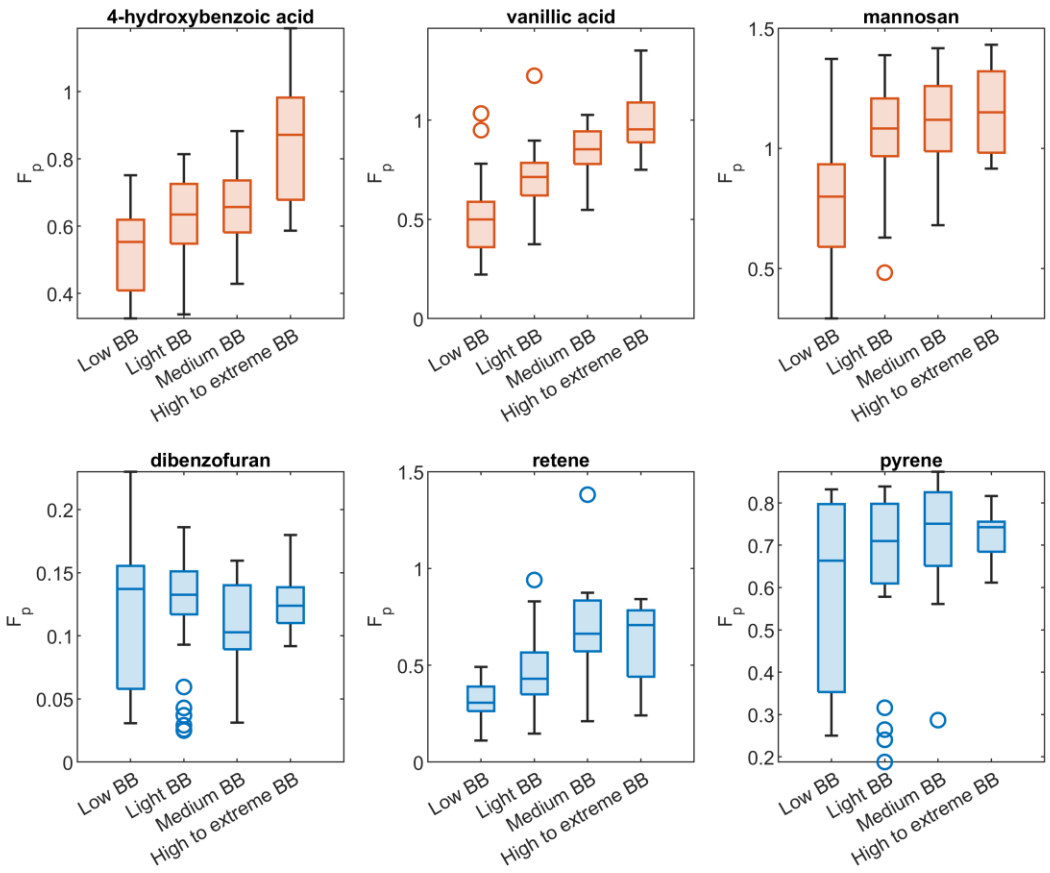

Figure S14. Boxplots showing the effect of BBOA on the particle phase fraction on selected compounds, observed in the FIREX-AQ 2018 study. Each box plot shows the interquartile range with whiskers extended to 1.5 × the interquartile range. Central horizontal lines show the medians. Circles denote outliers. BB influence categories are based on the concentration of particle phase levoglucosan. Low BB: 0-20th percentile; light BB: 20th-70th percentile, medium BB: 70th-90th percentile, high to extreme BB: above 90th percentile of levoglucosan concentration.

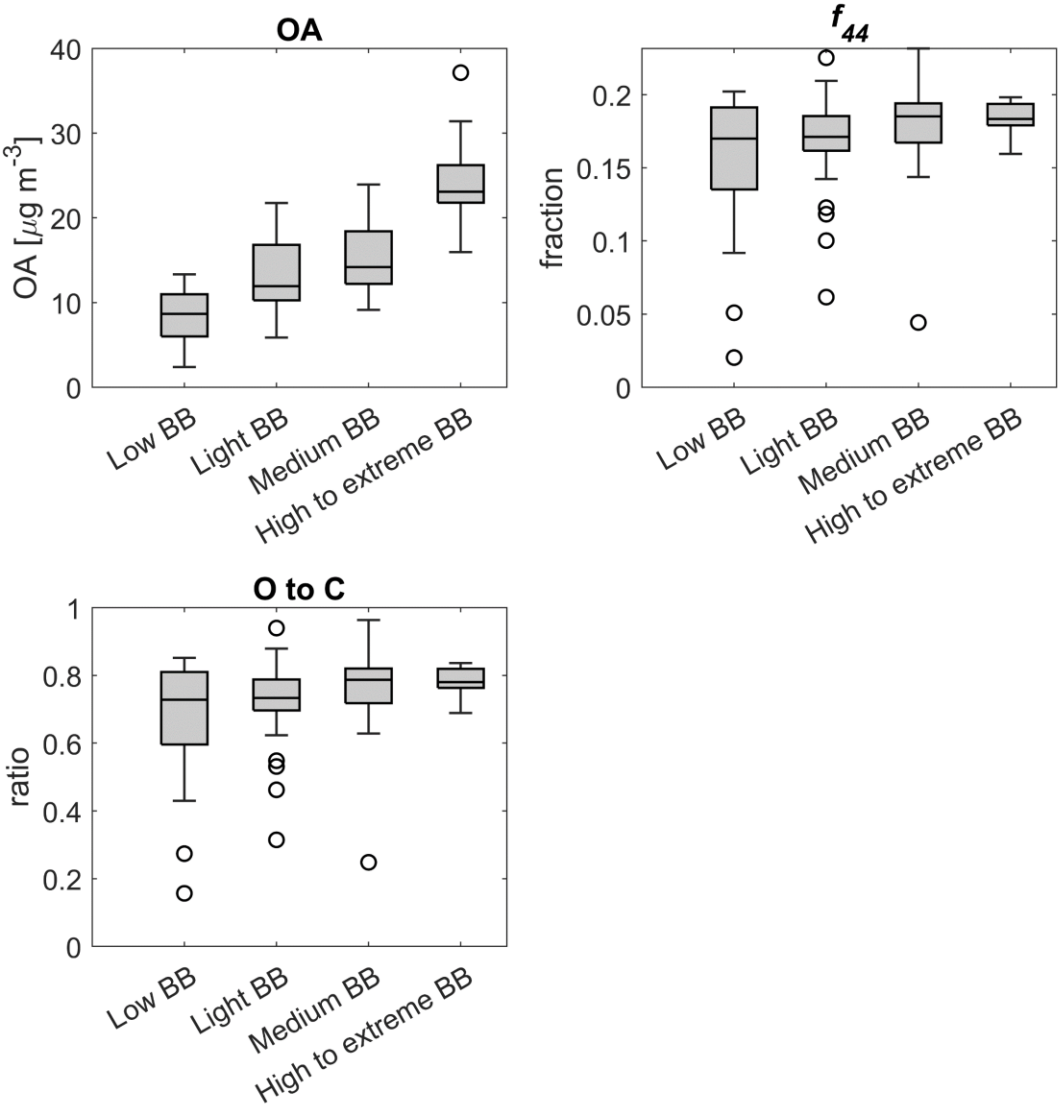

Figure S15. Boxplots showing the level of OA, f_{44}, and the estimated O/C ratio under different levels of biomass burning influence in the FIREX-AQ 2018 campaign.

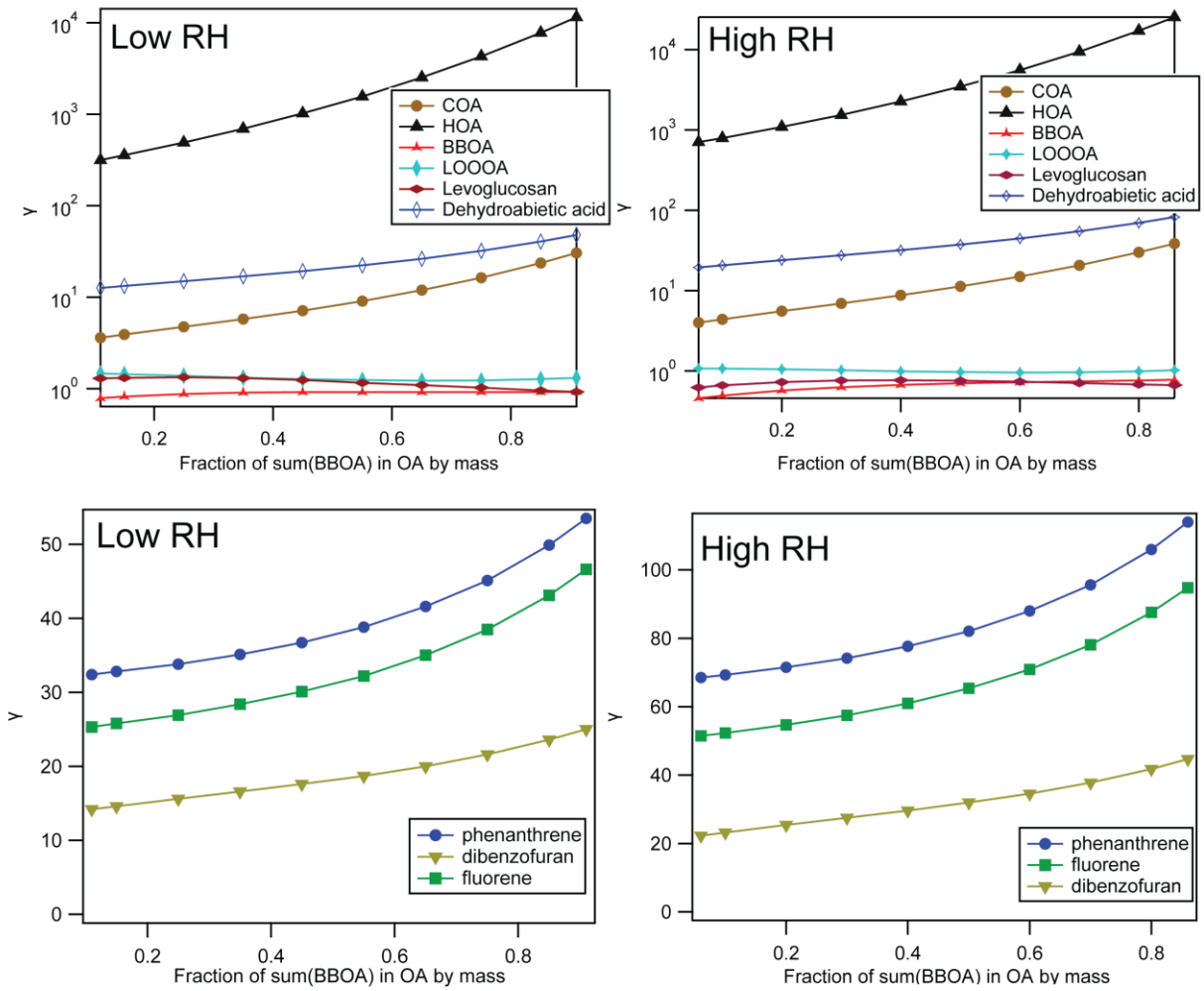

Figure S16. Predicted activity coefficients of aerosol components and selected compounds as functions of the fraction of the sum of BBOA components (BBOA without levoglucosan, levoglucosan and dehydroabietic acid), under low and high RH conditions described in Table S2.

References

Aiken, A. C., Decarlo, P. F., Kroll, J. H., Worsnop, D. R., Huffman, J. A., Docherty, K. S., Ulbrich, I. M., Mohr, C., Kimmel, J. R., Sueper, D., Sun, Y., Zhang, Q., Trimborn, A., Northway, M., Ziemann, P. J., Canagaratna, M. R., Onasch, T. B., Alfarra, M. R., Prevot, A. S. H., Dommen, J., Duplissy, J., Metzger, A., Baltensperger, U., and Jimenez, J. L.: O/C and OM/OC ratios of primary, secondary, and ambient organic aerosols with high-resolution time-of-flight aerosol mass spectrometry, Environ. Sci. Technol., 42, 4478–4485, https://doi.org/10.1021/es703009q, 2008.

Bannan, T. J., Booth, A. M., Jones, B. T., O'Meara, S., Barley, M. H., Riipinen, I., Percival, C. J., and Topping, D.: Measured Saturation Vapor Pressures of Phenolic and Nitro-aromatic Compounds, Environ. Sci. Technol., 51, 3922–3928, https://doi.org/10.1021/acs.est.6b06364, 2017.

Breiman, L.: Out-of-Bag Estimation, 1996.

Breiman, L.: Random Forests, Mach. Learn., 45, 5–32, https://doi.org/10.1023/A:1010933404324, 2001.

Compernolle, S., Ceulemans, K., and Müller, J. F.: Evaporation: A new vapour pressure estimation method for organic molecules including non-additivity and intramolecular interactions, Atmos. Chem. Phys., 11, 9431–9450, https://doi.org/10.5194/acp-11-9431-2011, 2011.

Engelhart, G. J., Hennigan, C. J., Miracolo, M. A., Robinson, A. L., and Pandis, S. N.: Cloud condensation nuclei activity of fresh primary and aged biomass burning aerosol, Atmos. Chem. Phys., 12, 7285–7293, https://doi.org/10.5194/ACP-12-7285-2012, 2012.

Epstein, S. A., Riipinen, I., and Donahue, N. M.: A Semiempirical Correlation between Enthalpy of Vaporization and Saturation Concentration for Organic Aerosol, Environ. Sci. Technol., 44, 743–748, https://doi.org/10.1021/es902497z, 2010.

Faber, P., Drewnick, F., Bierl, R., and Borrmann, S.: Complementary online aerosol mass spectrometry and offline FT-IR spectroscopy measurements: Prospects and challenges for the

analysis of anthropogenic aerosol particle emissions, Atmos. Environ., 166, 92–98, https://doi.org/10.1016/j.atmosenv.2017.07.014, 2017.

Fountoukis, C. and Nenes, A.: ISORROPIAII: A computationally efficient thermodynamic equilibrium model for K+-Ca2+-Mg2+-NH4+-Na+-SO42--NO3--Cl--H2O aerosols, Atmos. Chem. Phys., 7, 4639–4659, https://doi.org/10.5194/acp-7-4639-2007, 2007.

Guo, H., Xu, L., Bougiatioti, A., Cerully, K. M., Capps, S. L., Hite, J. R., Carlton, A. G., Lee, S. H., Bergin, M. H., Ng, N. L., Nenes, A., and Weber, R. J.: Fine-particle water and pH in the southeastern United States, Atmos. Chem. Phys., 15, 5211–5228, https://doi.org/10.5194/acp-15-5211-2015, 2015.

Isaacman-VanWertz, G., Yee, L. D., Kreisberg, N. M., Wernis, R., Moss, J. A., Hering, S. V, De Sá, S. S., Martin, S. T., Alexander, M. L., Palm, B. B., Hu, W., Campuzano-Jost, P., Day, D. A., Jimenez, J. L., Riva, M., Surratt, J. D., Viegas, J., Manzi, A., Edgerton, E., Baumann, K., Souza, R., Artaxo, P., and Goldstein, A. H.: Ambient Gas-Particle Partitioning of Tracers for Biogenic Oxidation, Environ. Sci. Technol., 50, 9952–9962, https://doi.org/10.1021/acs.est.6b01674, 2016.

Isaacman-VanWertz, G., Sueper, D. T., Aikin, K. C., Lerner, B. M., Gilman, J. B., de Gouw, J. A., Worsnop, D. R., and Goldstein, A. H.: Automated single-ion peak fitting as an efficient approach for analyzing complex chromatographic data, J. Chromatogr. A, 1529, 81–92, https://doi.org/10.1016/j.chroma.2017.11.005, 2017.

Isaacman, G., Kreisberg, N. M., Yee, L. D., Worton, D. R., Chan, A. W. H., Moss, J. A., Hering, S. V, and Goldstein, A. H.: Online derivatization for hourly measurements of gas- and particle-phase semi-volatile oxygenated organic compounds by thermal desorption aerosol gas chromatography (SV-TAG), Atmos. Meas. Tech., 7, 4417–4429, https://doi.org/10.5194/amt-7-4417-2014, 2014.

Jen, C. N., Hatch, L. E., Selimovic, V., Yokelson, R. J., Weber, R., Fernandez, A. E., Kreisberg, N. M., Barsanti, K. C., and Goldstein, A. H.: Speciated and total emission factors of particulate organics from burning western US wildland fuels and their dependence on combustion efficiency, Atmos. Chem. Phys., 19, 1013–1026, https://doi.org/10.5194/acp-19-1013-2019,

2019.

Kreisberg, N. M., Worton, D. R., Zhao, Y., Isaacman, G., Goldstein, A. H., and Hering, S. V.: Development of an automated high-temperature valveless injection system for online gas chromatography, Atmos. Meas. Tech., 7, 4431–4444, https://doi.org/10.5194/amt-7-4431-2014, 2014.

Liang, Y., Jen, C. N., Weber, R. J., Misztal, P. K., and Goldstein, A. H.: Chemical composition of PM2.5 in October 2017 Northern California wildfire plumes, Atmos. Chem. Phys., 21, 5719–5737, https://doi.org/10.5194/acp-21-5719-2021, 2021.

MathWorks: Predictor importance estimates by permutation of out-of-bag predictor observations for random forest of regression trees - MATLAB, 2022.

May, A. A., Saleh, R., Hennigan, C. J., Donahue, N. M., and Robinson, A. L.: Volatility of organic molecular markers used for source apportionment analysis: Measurements and implications for atmospheric lifetime, Environ. Sci. Technol., 46, 12435–12444, https://doi.org/10.1021/es302276t, 2012.

May, A. A., Levin, E. J. T., Hennigan, C. J., Riipinen, I., Lee, T., Collett, J. L., Jimenez, J. L., Kreidenweis, S. M., and Robinson, A. L.: Gas-particle partitioning of primary organic aerosol emissions: 3. Biomass burning, J. Geophys. Res. Atmos., 118, 11327–11338, https://doi.org/10.1002/jgrd.50828, 2013.

McGovern, A., Lagerquist, R., John Gagne, D., Jergensen, G. E., Elmore, K. L., Homeyer, C. R., and Smith, T.: Making the Black Box More Transparent: Understanding the Physical Implications of Machine Learning, Bull. Am. Meteorol. Soc., 100, 2175–2199, https://doi.org/10.1175/BAMS-D-18-0195.1, 2019.

Mecikalski, J. R., Sandmæl, T. N., Murillo, E. M., Homeyer, C. R., Bedka, K. M., Apke, J. M., and Jewett, C. P.: A Random-Forest Model to Assess Predictor Importance and Nowcast Severe Storms Using High-Resolution Radar–GOES Satellite–Lightning Observations, Mon. Weather Rev., 149, 1725–1746, https://doi.org/10.1175/MWR-D-19-0274.1, 2021.

Ng, N. L., Canagaratna, M. R., Jimenez, J. L., Chhabra, P. S., Seinfeld, J. H., and Worsnop, D.

R.: Changes in organic aerosol composition with aging inferred from aerosol mass spectra, Atmos. Chem. Phys., 11, 6465–6474, https://doi.org/10.5194/acp-11-6465-2011, 2011.

NIST Chemistry WebBook: https://webbook.nist.gov/, last access: 2 October 2022.

Pankow, J. F. and Asher, W. E.: SIMPOL.1: A simple group contribution method for predicting vapor pressures and enthalpies of vaporization of multifunctional organic compounds, Atmos. Chem. Phys., 8, 2773–2796, https://doi.org/10.5194/acp-8-2773-2008, 2008.

Pye, H. O. T., Zuend, A., Fry, J. L., Isaacman-VanWertz, G., Capps, S. L., Appel, K. W., Foroutan, H., Xu, L., Ng, N. L., and Goldstein, A. H.: Coupling of organic and inorganic aerosol systems and the effect on gas-particle partitioning in the southeastern US, Atmos. Chem. Phys., 18, 357–370, https://doi.org/10.5194/acp-18-357-2018, 2018.

Shah, R. U., Robinson, E. S., Gu, P., Robinson, A. L., Apte, J. S., and Presto, A. A.: High-spatial-resolution mapping and source apportionment of aerosol composition in Oakland, California, using mobile aerosol mass spectrometry, Atmos. Chem. Phys., 18, 16325–16344, https://doi.org/10.5194/acp-18-16325-2018, 2018.

Thornton, J. A., Mohr, C., Schobesberger, S., D'Ambro, E. L., Lee, B. H., and Lopez-Hilfiker, F. D.: Evaluating Organic Aerosol Sources and Evolution with a Combined Molecular Composition and Volatility Framework Using the Filter Inlet for Gases and Aerosols (FIGAERO), Acc. Chem. Res., 53, 1415–1426, https://doi.org/10.1021/acs.accounts.0c00259, 2020.

US EPA: Estimation Programs Interface Suite™ for Microsoft® Windows, 2012.

Wania, F., Awonaike, B., and Goss, K. U.: Comment on "measured Saturation Vapor Pressures of Phenolic and Nitro-Aromatic Compounds," Environ. Sci. Technol., 51, 7742–7743, https://doi.org/10.1021/acs.est.7b02079, 2017.

Yee, L. D., Isaacman-VanWertz, G., Wernis, R. A., Meng, M., Rivera, V., Kreisberg, N. M., Hering, S. V, Bering, M. S., Glasius, M., Upshur, M. A., Gray Bé, A., Thomson, R. J., Geiger, F. M., Offenberg, J. H., Lewandowski, M., Kourtchev, I., Kalberer, M., De Sá, S., Martin, S. T., Alexander, M. L., Palm, B. B., Hu, W., Campuzano-Jost, P., Day, D. A., Jimenez, J. L., Liu, Y., McKinney, K. A., Artaxo, P., Viegas, J., Manzi, A., Oliveira, M. B., De Souza, R., Machado, L.

A. T., Longo, K., and Goldstein, A. H.: Observations of sesquiterpenes and their oxidation products in central Amazonia during the wet and dry seasons, Atmos. Chem. Phys., 18, 10433–10457, https://doi.org/10.5194/acp-18-10433-2018, 2018.

Zhang, H., Yee, L. D., Lee, B. H., Curtis, M. P., Worton, D. R., Isaacman-VanWertz, G., Offenberg, J. H., Lewandowski, M., Kleindienst, T. E., Beaver, M. R., Holder, A. L., Lonneman, W. A., Docherty, K. S., Jaoui, M., Pye, H. O. T., Hu, W., Day, D. A., Campuzano-Jost, P., Jimenez, J. L., Guo, H., Weber, R. J., de Gouw, J., Koss, A. R., Edgerton, E. S., Brune, W., Mohr, C., Lopez-Hilfiker, F. D., Lutz, A., Kreisberg, N. M., Spielman, S. R., Hering, S. V., Wilson, K. R., Thornton, J. A., and Goldstein, A. H.: Monoterpenes are the largest source of summertime organic aerosol in the southeastern United States, Proc. Natl. Acad. Sci. U. S. A., 115, 2038–2043, https://doi.org/10.1073/pnas.1717513115, 2018.

Zhang, Q., Jimenez, J. L., Worsnop, D. R., and Canagaratna, M.: A case study of urban particle acidity and its influence on secondary organic aerosol, Environ. Sci. Technol., 41, 3213–3219, https://doi.org/10.1021/es061812j, 2007.

Zuend, A., Marcolli, C., Booth, A. M., Lienhard, D. M., Soonsin, V., Krieger, U. K., Topping, D. O., McFiggans, G., Peter, T., and Seinfeld, J. H.: New and extended parameterization of the thermodynamic model AIOMFAC: Calculation of activity coefficients for organic-inorganic mixtures containing carboxyl, hydroxyl, carbonyl, ether, ester, alkenyl, alkyl, and aromatic functional groups, Atmos. Chem. Phys., 11, 9155–9206, https://doi.org/10.5194/acp-11-9155-2011, 2011.